www.advenergymat.de

# Revealing the Role, Mechanism, and Impact of AIF<sub>3</sub> Coatings on the Interphase of Silicon Thin Film Anodes

Egy Adhitama, Stefan van Wickeren, Kerstin Neuhaus, Lars Frankenstein, Feleke Demelash, Atif Javed, Lukas Haneke, Sascha Nowak, Martin Winter, Aurora Gomez-Martin,\* and Tobias Placke\*

Silicon (Si) holds great promise as an anode material for high energy density lithium ion batteries owing to its theoretical capacity of up to 3579 mAh g<sup>-1</sup>. However, this potential comes at the expense of major challenges, because the solid electrolyte interphase (SEI) at Si anodes hardly provides long-term protection due to severe volume expansion. Yet, when it comes to the SEI, the formation mechanism is not thoroughly understood. Here, thin AIF<sub>3</sub> coatings are deposited on Si thin film to stabilize the SEI. To evaluate the SEI, systematic observation utilizing X-ray photoelectron spectroscopy is performed at different (de-)lithiation states, allowing stage-by-stage analysis to reveal the role, mechanism, and impact of AIF3 coating. Results show that the capacity retention is significantly improved for 90% after 100 cycles. The transformation of AIF<sub>3</sub> into Li-Al-F compounds, as confirmed by ion chromatography, is responsible for an enhanced performance due to its high ionic conductivity. Moreover, the SEI of coated Si thin films is rich in inorganic species (i.e., LiF) which is beneficial to prevent electrons to pass through. This work will deepen the understanding of SEI on Si anodes with respect to the coating approach, suggesting future directions to improve coating layers on Si.

E. Adhitama, S. Wickeren, L. Frankenstein, F. Demelash, A. Javed, L. Haneke, S. Nowak, M. Winter, A. Gomez-Martin, T. Placke University of Münster

MEET Battery Research Center Institute of Physical Chemistry

Corrensstr. 46, 48149 Münster, Germany

E-mail: agomezma@uni-muenster.de; tobias.placke@uni-muenster.de

E. Adhitama, A. Javed University of Münster

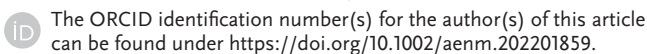
International Graduate School for Battery Chemistry Characterization

Analysis Recycling and Application (BACCARA)

Corrensstr. 40, 48149 Münster, Germany

K. Neuhaus, M. Winter Helmholtz Institute Münster IEK-12

Forschungszentrum Jülich GmbH Corrensstr. 46, 48149 Münster, Germany



© 2022 The Authors. Advanced Energy Materials published by Wiley-VCH GmbH. This is an open access article under the terms of the Creative Commons Attribution License, which permits use, distribution and reproduction in any medium, provided the original work is properly cited.

DOI: 10.1002/aenm.202201859

#### 1. Introduction

The development of efficient electrochemical energy storage devices will ease the transition toward a carbon-free society and is the key to a more sustainable energy supply and use.[1] In the last 30 years, lithium ion batteries (LIBs) have been extensively explored, however, better performance in terms of higher energy content and lower production costs is still required to fulfill future needs for highly demanding applications, such as electro-mobility.[2] In this respect, there is still room for further improvements, as silicon (Si) holds greater promise as an anode material compared to state-ofthe-art (SOTA) graphite materials due to the almost 10-fold increase in specific capacity, low delithiation potential (≈0.4 V vs. Li|Li+), and low-cost precursor materials.[3] Si experiences a series of phase transitions when alloying with Li (formation of several intermetallic phases),

offering a maximum gravimetric capacity of 3579 mAh g $^{-1}$  for the Li $_{15}$ Si $_4$  phase. $^{[4]}$  Despite the perceived advantages, the commercialization of Si-rich (the so-called Si-dominant) anodes for high-energy LIB cells is still challenging. Si suffers from a huge volume expansion during lithiation/delithiation processes, resulting in irreversible changes in particle morphology and size. $^{[5]}$  In such conditions, the ineffective solid electrolyte interphase (SEI) fails in preventing parasitic reactions at the Si|electrolyte interface during operation and, thus, does not prevent continuous electrolyte reduction and active lithium consumption. $^{[6]}$ 

When the electrolyte is brought to potentials outside its electrochemical stability window, the electrolyte components react at the electrode|electrolyte interfaces, which results in the interphase formation, e.g., SEI formation at the anode active material surface. For instance, the typical operation potential of the Si anodes in LIBs is  $\approx\!0.01\text{--}1.00~\text{V}$  versus Li|Li<sup>+</sup>. At such low potentials, SOTA carbonate-based electrolytes are unstable and are electrochemically reduced at the anode surface forming a thin film, i.e., the so-called SEI. Despite more than 20 years of advanced study in this area, the SEI, however, remains "the most important and the least understood" aspect of LIB cells. [9]

ADVANCED ENERGY MATERIALS

www.advancedsciencenews.com

Previous studies aiming at understanding passivation film formation agree that the SEI should permit the diffusion of Li<sup>+</sup> ions while being impermeable for solvent molecules and preventing the penetration of electrons.<sup>[10]</sup> In fact, the SEI at Si anodes is doubtful to continuously protect the active materials in SOTA carbonate-based electrolytes unlike what it does for graphite anodes.[11] While SEI formation on graphite anodes is normally completed after the first few charge/discharge cycles in a LIB cell, the drastic structural disruption (e.g., crystallization and amorphization) during (de-)lithiation in Si anodes causes cracking of particles, leading to ongoing electrolyte reduction and SEI breakage/(re-)formation. This eventually increases the internal resistance of the cell, electrolyte consumption (drying out), and the consumption of Li+ ions stemming from the cathode.<sup>[12]</sup> Only when a highly effective SEI is formed, continuous electrolyte reduction at low potentials is prevented and, hence, the Coulombic efficiency ( $C_{\text{Eff}}$ ) and reversible capacity will be improved. [6b]

To prevent continuous electrolyte reduction and enable effective SEI formation, tremendous efforts have already been proposed. Fluoroethylene carbonate (FEC) has been widely used as an SEI-forming electrolyte additive[13] or even as a single solvent[14] to form an effective SEI on Si anodes. However, once all the FEC is consumed, the LIB cell will experience a sudden failure with a rapid capacity decay.<sup>[15]</sup> Another strategy is by employing an organic or inorganic coating layer on the surface of Si. [16] The terms "artificial" SEI [17] or protective surface coating<sup>[18]</sup> are oftentimes used to describe the role of this layer. In Si anodes, coating layers are often designed to shield the reactive Li<sub>x</sub>Si<sub>y</sub> phase during the alloying process from direct contact with the electrolyte. Furthermore, the functional coating layer also has to be (electro)chemically and mechanically stable enough to withstand battery operation without degradation, while maintaining a low resistance for Li<sup>+</sup> ion diffusion. However, the maximum exploration of its benefits is still hampered by the inability to predict and control its multifunctionality as an electronic insulator and an ionic conductor.

Oxides (e.g., Al<sub>2</sub>O<sub>3</sub>, MgO, TiO<sub>2</sub>)<sup>[19]</sup> and fluorides (e.g., LaF<sub>3</sub>, MgF<sub>2</sub>, AlF<sub>3</sub>)<sup>[20]</sup> are two classes of materials that have been widely studied as surface coating materials for LIB layered cathodes (e.g., LiNi<sub>x</sub>Co<sub>v</sub>Mn<sub>z</sub>O<sub>2</sub> (NCM-xyz), LiCoO<sub>2</sub>, LiNiO<sub>2</sub>, and LiMnO<sub>2</sub>) to minimize parasitic side reactions at the electrode|electrolyte interface. Oxides are generally reported to improve cycling stability although there is still a debate to what degree the coating can significantly mitigate oxygen loss from the lattice.[19a,21] Fluorides are believed to be beneficial to enhance electrochemical performance by acting as HF scavengers and suppressing electrolyte decomposition. The enhanced performance of fluoride-based coatings was tentatively attributed to its function as a "buffer" layer. [20c] After all, the fact that these inorganic coatings improve the physical properties and/or cycling stability is unquestionable, but the working principle remains not well understood. To take full advantage of these inorganic coatings, it is vital to understand their role not only from the electrochemical outcomes but rather to elucidate their mechanism during electrochemical cycling to justify the use of such surface coatings. Among fluoride materials, AlF3 is one of the most commonly used coatings on cathode active material particles. The Li+ transport through AlF3 surface coatings on the

www.advenergymat.de

cathode has been thoroughly evaluated. [22] It has been reported that the AlF<sub>3</sub> coating layer facilitates Li<sup>+</sup> ion movement once it has been lithiated. [23] By nature, the Li<sup>+</sup> diffusivity in AlF<sub>3</sub> is low (1.1  $\times$  10<sup>-13</sup> m² s<sup>-1[22b]</sup>), however, it is found that Li—Al—F bonds exist in lithiated AlF<sub>3</sub>, making it a stable Li-conducting solid electrolyte (e.g., Li<sub>3</sub>AlF<sub>6</sub> with ionic conductivity of 10<sup>-6</sup> S cm<sup>-1[24]</sup> or LiAlF<sub>4</sub> with 10<sup>-4</sup> S cm<sup>-1,[25]</sup> respectively). Thus, it allows Li<sup>+</sup> ions to exchange at the interface due to its low charge transfer resistance. [24] However, the influence of AlF<sub>3</sub> coatings on the anode has been barely studied so far. Based on our understanding, only a few studies have investigated the impact of AlF<sub>3</sub> on the anodes [23,26] but the mechanism remains elusive.

In this work, a systematic evaluation of how AlF<sub>3</sub> as surface coating mediates the composition of the SEI formed on Si anodes as a function of the (de-)lithiation state is provided. Si thin films were used as a model system to neglect binder and conductive agent interference. Two different thicknesses of 5 nm (further referred to as "Si + 5 nm AlF<sub>3</sub>") and 20 nm (further referred to as "Si + 20 nm  $AlF_3$ ") of the  $AlF_3$  layer were deposited on top of Si thin films. It is worth noting that the conditions of the electrode with and without coating are chemically not equivalent. Consequently, the chemical stability, insulating property, and ionic conductivity of the AlF<sub>3</sub> layer are considered to be important. Thus, three key questions arise: i) "What is the mechanism for the possible phase transformation of AlF<sub>3</sub>?" ii) "How does the AlF3 coating layer influence SEI formation on Si anodes?" and iii) "What is the effect of the layer on the C<sub>Eff</sub>, active lithium losses, and capacity fading?" In this work, we demonstrate that AlF<sub>3</sub> coating is feasible for Si thin film anodes and provide deeper insights into SEI formation by utilizing X-ray photoelectron spectroscopy (XPS) in different (de-) lithiation states combined with an ion chromatography with conductivity detection (IC-CD). This study shall provide extensive insights into the SEI behavior with regard to the functional coating layer, and thus suggests future directions to advance studies of the coating layers on Si anodes.

#### 2. Results and Discussion

#### 2.1. Structural Characterization of Si Thin Film Electrodes

Si thin films of different thicknesses (100-300 nm) were deposited on smooth copper foil via magnetron sputtering (see the Experimental Section in the Supporting Information for further details). The crystallinity of the as-deposited Si was first evaluated using X-ray diffraction (XRD). The XRD pattern does not show any reflections of crystalline Si. Instead, very intense Cu reflections and a small hump at low diffraction angles are present, indicating that the as-deposited Si thin film has an amorphous character, as seen in Figure S1 (Supporting Information). The thickness of amorphous Si (a-Si) layers on the Cu substrate was then verified using scanning electron microscopy (SEM) with a focused-ion beam (FIB) technique. The Si thin films were successfully deposited with thicknesses of ≈100, ≈200, and ≈300 nm, as shown in Figure S2a-c (Supporting Information). The top view SEM images of the pristine Si electrodes are depicted in Figure 1a-c, displaying no significant differences.

16146840, 2022, 41, Downloaded from https://onlinelibrary.wiley.com/doi/10.1002/aenna.202201859 by Forschungszentrum Jülich GmbH Research Center, Wiley Online Library on [04/11/2022]. See the Terms and Conditions (https://onlinelibrary.wiley.com/terms-and-

conditions) on Wiley Online Library for rules of use; OA articles are governed by the applicable Creative Commons

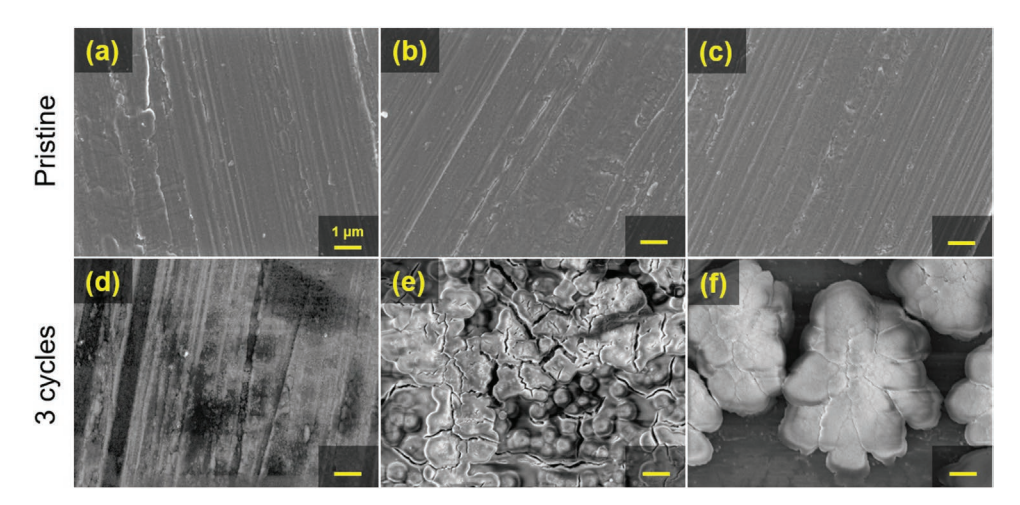


Figure 1. Top view SEM micrographs of Si thin films with different thicknesses in a pristine state a–c) and after three charge/discharge cycles d-f: a,d) 100 nm, b,e) 200 nm, c,f) 300 nm. Top images correspond to pristine electrodes, while bottom images correspond to cycled electrodes. The scale bar corresponds to 1  $\mu$ m for all micrographs.

Si thin film electrodes were then electrochemically evaluated in Si || Li metal cells using constant current charge/ discharge cycling at a rate of 0.1C, as depicted in Figure S3a (Supporting Information). The initial  $C_{\text{Eff}}$  values after 3 formation cycles are 92%, 95%, and 98% for 100, 200, and 300 nm Si thin film anodes, respectively. As the number of cycles increased, a decline in specific capacity was observed for all cells. Among the three materials, the thinnest (100 nm) Si thin film cells yield the most stable performance, while the thickest (300 nm) exhibit the worst cycling stability, in agreement with previous findings.<sup>[27]</sup> Interestingly, 100 nm Si-based cells show the highest accumulated Coulombic inefficiency (ACI)<sup>[28]</sup> while 300 nm Si-based cells show the lowest value, as illustrated in Figure S3b (Supporting Information). The contradictory result between capacity retention and ACI could possibly originate from a higher ratio of the surface area to mass in the 100 nm Si thin film anodes, which, by reaction with the electrolyte, traps more Li+ ions in the SEI as compared to the 300 nm Si thin film anodes. In the case of thick(er) Si thin film anodes, the partial activation and mechanical degradation upon cycling cause significant compressive stress leading to pulverization of active material and thus an abrupt capacity loss (e.g., in 300 nm Si cells, the capacity is already significantly reduced after  $\approx$ 20 cycles). [29] As a result, the thinner Si film exhibits the lowest capacity fading but the highest ACI value.

These different mechanical degradation phenomena of the Si thin films after 3 charge/discharge cycles are depicted in the SEM micrographs in Figure 1d–f. A rather smooth surface was detected for 100 nm Si thin film electrodes, while visible microcracks with voids between Si materials were noticed for 200 nm Si thin film electrodes. In contrast, the Si active materials were detached from the current collector in the 300 nm thin film electrodes, which might be the origin of the sudden capacity drop. Considering these results, 100 nm thick Si thin films will be used in all further sections due to their higher stability.

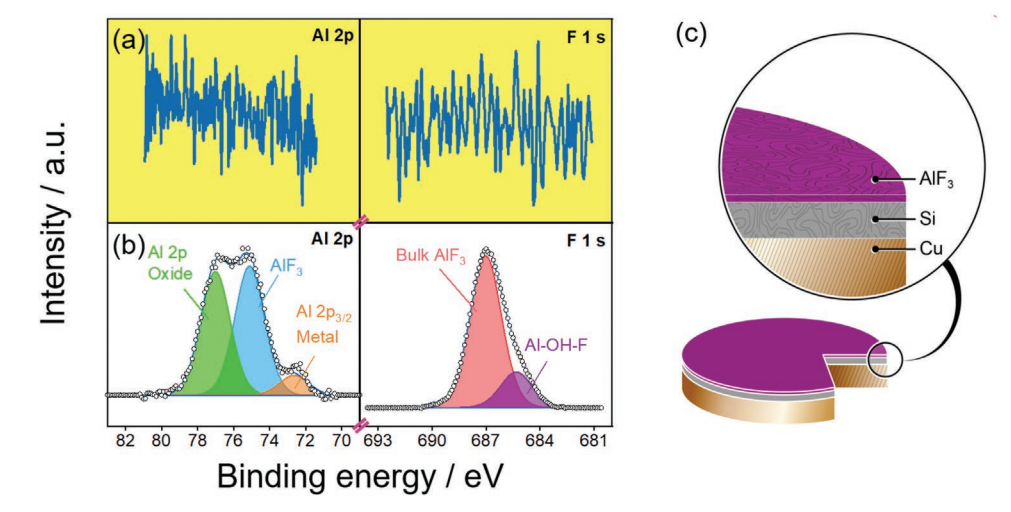


Figure 2. Al 2p and F 1s XPS core spectra for a) uncoated Si thin film, and b) coated Si thin film (Si + 20 nm AlF<sub>3</sub>). The annotated compounds are displayed. c) Schematic illustration of AlF<sub>3</sub> coated on top of Si thin film electrodes.

conditions) on Wiley Online Library for rules of use; OA articles are governed by the applicable Creative Commons

ADVANCED ENERGY

www.advancedsciencenews.com www.advenergymat.de

## 2.2. Characterization of AIF<sub>3</sub> Coatings on Top of Si Thin Film Electrodes

Thin layers of AlF<sub>3</sub> with a thickness of 5 nm ("Si + 5 nm AlF<sub>3</sub>") and 20 nm ("Si + 20 nm AlF<sub>3</sub>") were deposited on top of Si thin films. The successful AlF3 coating on Si thin film electrodes was confirmed by means of XPS, as representatively shown for the "Si + 20 nm AlF<sub>3</sub>" electrodes in Figure 2b. In Figure 2a, no F 1s and Al 2p peaks exist in uncoated Si thin film electrodes. In contrast, the F 1s and Al 2p spectra display a very intense peak for the coated Si thin film, thus, revealing the presence of F and Al atoms with an atomic concentration of ≈29 and ≈24 at%, respectively (Figure 2b). The surface composition of both spectra primarily corresponds to AlF<sub>3</sub>. Al 2p spectra show a contribution from oxygen which reacts immediately with Al forming Al<sub>2</sub>O<sub>3</sub> once the samples are exposed to air.<sup>[30]</sup> In the F 1s spectra, bulk AlF<sub>3</sub> is supposed to be centered at a binding energy (BE) of ≈686.8 eV, as reported in the literature. [31] The existence of a peak at lower BEs (at ≈685 eV) is associated with aluminum oxyfluoride species.<sup>[32]</sup> Sputter depth profiling was further employed with 4 kV Ar<sup>+</sup> ions and both Al and F signals strongly decrease after 240 s. At the same time, the weak intensity of the initial Si 2p peak became stronger after the sputtering process is done (Figure S4a-c, Supporting Information). The evolution of the F 1s, Al 2p, and Si 2p spectra as a function of the sputtering time demonstrates the successful existence of a thin AlF3 layer on top of the Si film electrode, as schematically illustrated in Figure 2c.

Further, the samples were evaluated by atomic force microscopy (AFM) technique, namely Kelvin probe force microscopy (KPFM). In general, AFM is a frequently used method for determining the topography of a given sample and KPFM is an AFM-based method that enables the determination of the local surface potential in combination with the sample topography.<sup>[33]</sup> The surface potential is sensitive to the defect concentration at the outermost surface of the samples and it correlates to local electron transport properties. [34] In this matter, KPFM measurements can provide insightful information about the condition of these properties at the electrode interface. Figure 3a,b displays the surface topography determined by AFM of uncoated and AlF<sub>3</sub>-coated Si thin films, respectively. Both samples show a rather smooth surface morphology where the observable lines emerge from the used copper foil. The uncoated Si thin films have a root mean square (RMS) surface roughness of ≈102 nm, whereas the value for coated Si thin film is ≈108 nm. These similar values imply that the coating of AlF<sub>3</sub> does not significantly affect the morphology of Si thin films. Moreover, these values are considerably small, so the Si thin film electrodes have a better ability to avoid the risk of local overcharge (or over-discharge) which is hardly achieved for porous Si or Si/graphite composite electrodes. Figure 3c,d shows the local surface potential determined by KPFM of uncoated and coated Si thin films, respectively. The figures show that notable differences exist in the surface potential of the sample after the addition of the AlF<sub>3</sub> layer. A significant increase in the surface potential for the coated Si thin films (≈0.1–0.3 V) in comparison

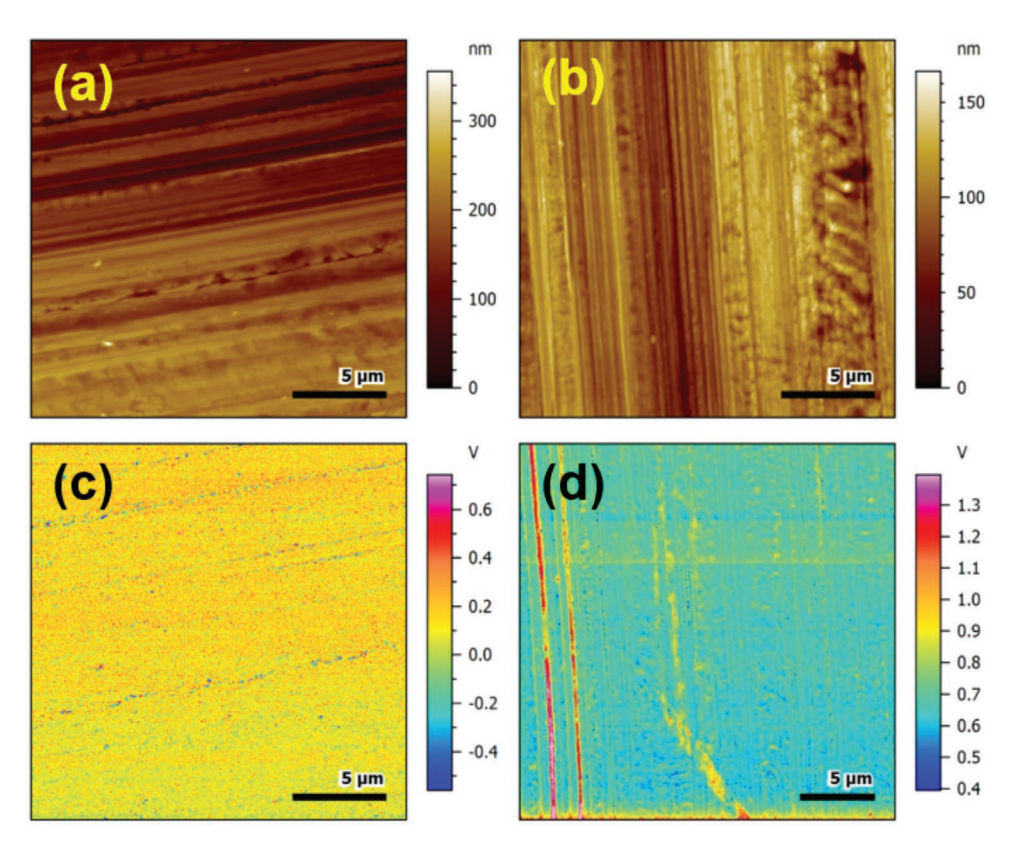


Figure 3. Topography evaluation using AFM of pristine a) uncoated Si thin film and b) coated Si thin film electrodes. Surface potential images of c) uncoated Si thin film and d) coated Si thin film electrodes measured by KPFM technique.

ADVANCED ENERGY MATERIALS

www.advancedsciencenews.com www.advenergymat.de

to uncoated Si thin films ( $\approx$ 0.7–0.9 V) confirms the nature insulating properties of the AlF<sub>3</sub> coating. The increase of the surface potential can be considered as a decreased tendency for electron transfer<sup>[35]</sup> which is a favorable feature of an effective SEI.

## 2.3. Electrochemical Performance Evaluation of Si Thin Film Electrodes

Figure 4a compares the first lithiation behavior of Si thin films, "Si + 5 nm AlF<sub>3</sub>," and "Si + 20 nm AlF<sub>3</sub>," respectively. Similar features were observed in the voltage profile of all cells except a small potential spike at 0.8 V for "Si + 20 nm AlF<sub>3</sub>" (see the inset). This feature is possibly due to a single-phase transition of AlF<sub>3</sub> to form Li-Al-F bonds.<sup>[24]</sup> This voltage spike can also be seen in the first cycle (at  $\approx 0.8$  V) in the dQ/dV profiles as depicted in Figure 4b,c. In general, the peak positions of the first cyclic voltammetry (CV) scan for all cells are relatively similar which suggests that the AlF<sub>3</sub> coating does not significantly affect the lithiation mechanism and possibly does not contribute to the suppression of structural change as the formation of Li<sub>x</sub>Si<sub>v</sub> still takes place reversibly. The slight difference between these cells from CV measurements is that the current peaks during lithiation in uncoated Si thin film cells are a bit larger, which indicates faster kinetics leading to a higher degree of lithiation than in coated Si thin films. During delithiation, the current peaks of the uncoated Si thin film are not as large as the lithiation peaks, implying worse reversibility as compared to coated Si thin film since the peak ratio between lithiation and delithiation is seemingly relatively smaller (Figure 4c).

The impact of AlF<sub>3</sub> on SEI formation was further investigated by taking a closer look at the attainable specific capacity in the first cycle for the different cells. The first lithiation capacity for uncoated Si is ≈5440 mAh g<sup>-1</sup> (Figure 4d). It decreases with the addition of AlF<sub>3</sub> film to ≈5100 mAh g<sup>-1</sup> for both "Si + 5 nm  $AlF_3$ " and "Si + 20 nm  $AlF_3$ " electrodes, respectively. The delithiation capacity of uncoated Si thin film electrodes (≈3290 mAh g<sup>-1</sup>) is lower compared to those of "Si + 5 nm AlF<sub>3</sub>" and "Si + 20 nm AlF<sub>3</sub>" ( $\approx$ 3600 mAh g<sup>-1</sup>). These values correspond to  $C_{\rm Eff}$  of 60.5% and 70.6% for the uncoated and coated Si thin film cells, respectively. The enhancement of C<sub>Fff</sub> for the coated Si thin film cells suggests that the SEI formed under the influence of AlF<sub>3</sub> film is more effective and leads to better reversibility. Noteworthy, it remains a question why the first lithiation capacity in every Si thin film anode case is always higher than the theoretical capacity of Si (each Si atom is practically only able to uptake as many as 3.75 Li atoms (Li<sub>15</sub>Si<sub>4</sub> phase) at room temperature which leads to a capacity of  $\approx 3579$  mAh g<sup>-1</sup>). It has been reported elsewhere[36] including from the early studies on Si thin films, [37] however, the origin of the high first lithiation capacity (= poor  $C_{\text{Eff}}$ ) has not been deeply discussed or is simply justified due to the formation of the SEI on the surface of Si thin films (e.g., the additional capacity from the irreversible reduction of salt and solvent molecules during SEI formation to the practical capacity of Si thin films).

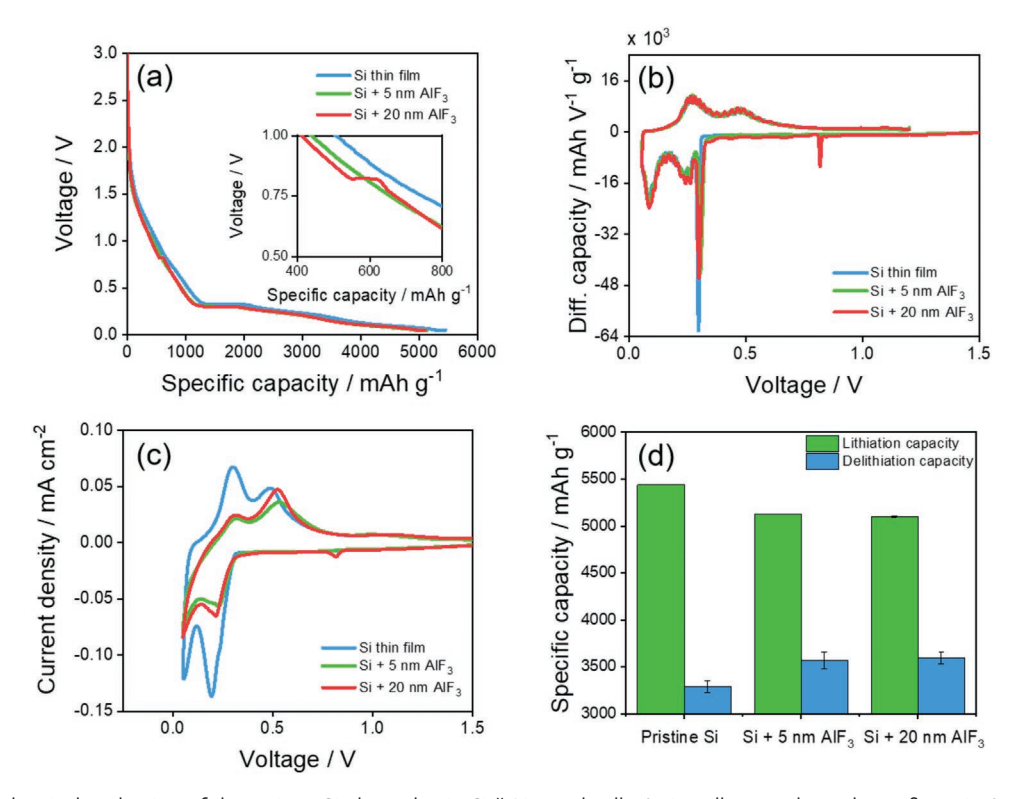


Figure 4. Electrochemical evaluation of the various Si electrodes in Si  $\parallel$  Li metal cells (coin cells, two-electrode configuration). a) First discharge (= lithiation) voltage profiles at 0.1C. b) First cycle differential capacity (dQ/dV) versus voltage curves at 0.1C. c) Cyclic voltammetry profiles at a scan rate of 25  $\mu$ V s<sup>-1</sup> in a voltage range between 0.05 and 1.5 V and d) First cycle lithiation/delithiation capacities at 0.1C for the different materials. The error bars represent the standard deviation of at least three cells.

xonditions) on Wiley Online Library for rules of use; OA articles are governed by the applicable Creative Commons License

www.advancedsciencenews.com

ADVANCED ENERGY MATERIALS

www.advenergymat.de

Further, the impedance characterization supports that some structural changes have occurred to the AlF<sub>3</sub> coating, which facilitates Li<sup>+</sup> ion transport. Electrochemical impedance spectroscopy (EIS) measurements were performed on all cells after 1 formation cycle. The Nyquist plots (Figure S5a,b, Supporting Information) present a semicircle for all cells. It is found that the charge transfer resistance is notably reduced by the AlF<sub>3</sub> coating. The charge transfer resistance for uncoated Si, "Si + 5 nm  $AlF_3$ ," and "Si + 20 nm  $AlF_3$ " is 339.8, 184.2, and 176.8  $\Omega$ , respectively, and it does not significantly change in each of the (de-)lithiation states. The lower resistance value of coated Si thin film anodes is an indication that the AlF<sub>3</sub> film is going through a formation process where an insulating AlF<sub>3</sub> can be activated to become ionically conductive after the lithiation process, as previously reported.<sup>[24]</sup> Thus, the formed interphase helps Li<sup>+</sup> to diffuse into the Si thin films and therefore causes a lower charge transfer resistance. The trend of these values is remarkably consistent even after 100 cycles (Figure S5c,d, Supporting Information). The mechanism will be discussed further in the next section with support from XPS and IC-CD results.

CV profiles shown in Figure S6a–c (Supporting Information) highlight the current peaks related to SEI formation, kinetics, and (de-)lithiation processes. In the uncoated Si thin film cells, the difference between the first lithiation peak compared to the second and further cycles is due to SEI formation (Figure S6a, Supporting Information). For delithiation peaks, similar characteristics from the first to further cycles were observed. With the addition of AlF3, a noticeably shifted first (de-)lithiation peaks were detected (e.g., see the green dotted lines which show that the delithiation peak of the first cycle at  $\approx\!0.53$  V was different in comparison to the second and further cycles at  $\approx\!0.50$  V as shown Figure S6b,c, Supporting Information), suggesting the AlF3 influences SEI formation and kinetics for (de-)lithiation. The CV curves are in good agreement with the EIS profiles.

In **Figure 5**a–f, the cycling performance over 100 cycles of uncoated Si thin film, "Si + 5 nm AlF<sub>3</sub>," and "Si + 20 nm AlF<sub>3</sub>"

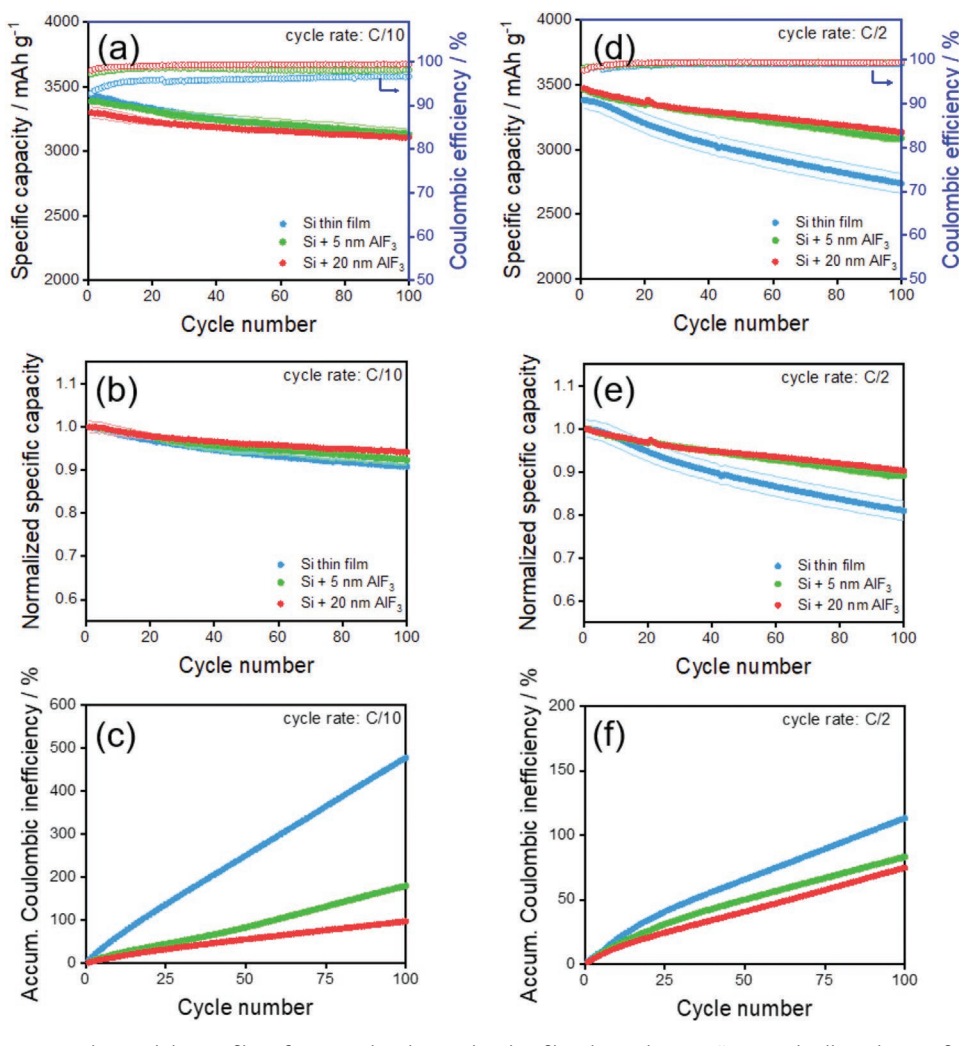


Figure 5. Constant current cycling stability profiles of uncoated and coated Si thin film electrodes in Si  $\parallel$  Li metal cells. a,d) Specific capacity versus cycle number profiles. b,e) Normalized specific capacity (based on initial de-lithiation capacity) versus cycle number profiles. c,f) Accumulated Coulombic inefficiency (ACI) profiles. Cells in a–c) were cycled at C/10, while cells in d–f) were cycled at C/2 (1C = 3000 mA g<sup>-1</sup>). Standard deviations from three cells per sample are included.

www.advancedsciencenews.com

**ENERG** 

are compared. In Figure 5a, the stability performances at C/10 (1C = 3000 mAh  $g^{-1}$ ) of all electrodes are seemingly similar. If one takes a look at the normalized long-term cycling profiles (based on the first delithiation capacity) shown in Figure 5b, the reversibility of coated Si thin films (i.e., "Si + 5 nm AlF<sub>3</sub>" and "Si + 20 nm AlF<sub>3</sub>") is slightly better than uncoated Si thin films. A more clear trend can be seen in Figure 5c where the ACI of coated Si thin films is significantly lower than that of coated Si thin films.

The effect of AlF<sub>3</sub> coating was then evaluated at a higher current rate of C/2. Clearly, the coated Si thin films display a more stable and higher reversible capacity of ≈400 mAh g<sup>-1</sup> after 100 cycles as compared to uncoated Si thin film cells (Figure 5d). This is equal to ≈90.2% of capacity retention for the coated Si thin film cells while only ≈80.9% for uncoated Si thin film cells which can be seen from the normalized capacity profiles in Figure 5e. These trends are in agreement with ACI profiles shown in Figure 5f, where coated Si thin films show notably lower value in comparison to uncoated Si thin films. The excellent cycling performance of coated Si thin films can be attributed to the AlF<sub>3</sub> coating, resulting in a more effective and stable SEI that is able to better passivate Si active material during (de-) lithiation as well as partially shields the electrolyte from the reactive Li<sub>x</sub>Si<sub>y</sub> surface.

#### 2.4. SEI Investigations on Si Thin Film Electrodes by XPS **Analyses**

The composition of the SEI has a critical effect on the cycling stability of Si anodes, [39] and XPS is the commonly employed technique for identifying its chemical composition.<sup>[39a,40]</sup> It is important to note that XPS samples should be handled appropriately as it is a surface-sensitive technique. [41] In this study,

the cycled electrodes (from the 1st charge/discharge cycle) were washed using dimethyl carbonate (DMC) before being transferred to the XPS chamber to avoid potential Li salt interference during XPS measurements. From now on, the term coated electrodes only correspond to "Si + 20 nm AlF<sub>3</sub>." "Si + 5 nm AlF<sub>3</sub>" is not discussed here since the electrochemical data shown in Figure 5a-e is comparable to that of "Si + 20 nm AlF<sub>3</sub>" and thus no significant differences in the SEI composition are expected.

www.advenergymat.de

As shown in Figure S7a-f (Supporting Information), the sputter depth profiling technique is conducted to gain qualitative information about the thickness of the chemical products on coated and uncoated Si thin films as a function of (de-) lithiation states. Figure 6a,b and Figure S8a,b (Supporting Information) depict the XPS spectra and corresponding fits for F 1s and C 1s spectra for uncoated and AlF3-coated Si thin films. The measurements were taken during lithiation with voltage holds at 0.8, 0.2, 0.05 V and during delithiation at 0.2 V. A more detailed discussion can be found in Note S2 in the Supporting Information.

In general, the LiF (≈685 eV) fraction in uncoated Si thin film electrodes is lower than the fraction of LiPF<sub>6</sub>/Li<sub>x</sub>PO<sub>v</sub>F<sub>z</sub> (≈687 eV) species in all (de-)lithiation states (Figure 6a; and Figure S9a, Supporting Information). In contrast, the coated Si electrodes show a significantly higher fraction of LiF species than the fraction of LiPF<sub>6</sub>/Li<sub>x</sub>PO<sub>v</sub>F<sub>z</sub> species in all (de-) lithiation states (Figure 6b; and Figure S9b, Supporting Information). This is attributed to the transformation of AlF<sub>3</sub> to LiF and Li-Al-F (≈686 eV<sup>[42]</sup>) compounds. It is reported that Li-Al-F compounds shall possess excellent Li+ ion conductivity due to the partially occupied Li<sup>+</sup> ion sites inside.<sup>[25a]</sup> The existence of Li-Al-F help in reducing the energy barriers for Li+ ion insertion and enhance the charge transfer kinetics. A similar observation was reported by Wang et al.[43] who stated that the presence of AlF<sub>3</sub> is beneficial for improving the ionic

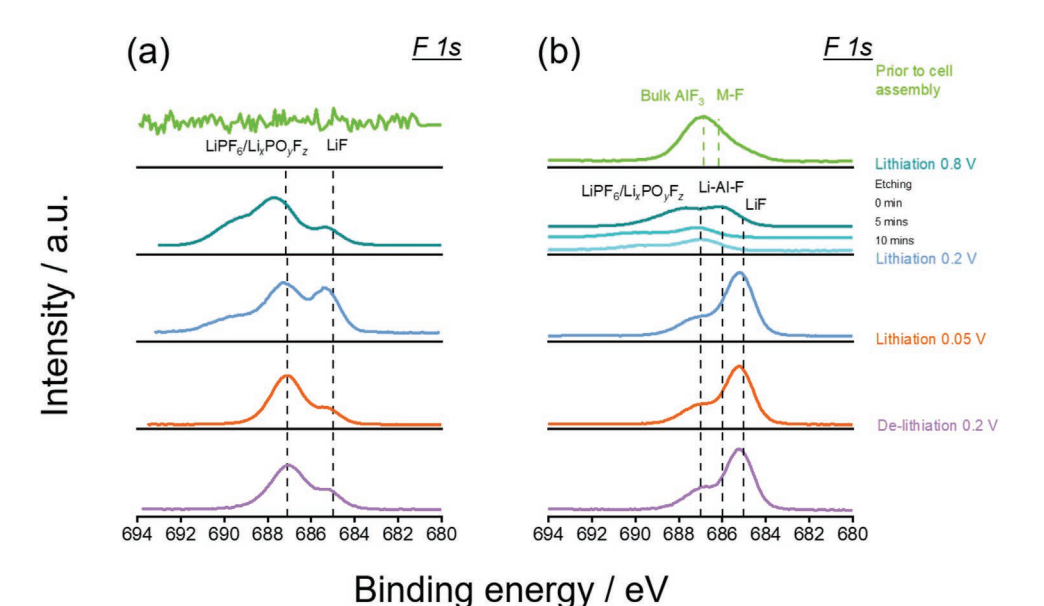


Figure 6. XPS core spectra of the F 1s: a) uncoated Si, and b) 20 nm AIF<sub>3</sub>-coated Si thin films. The XPS results prior to cell assembly and after cycling to different (de-)lithiation states in the first cycle are shown. The cycled samples are held at 0.8, 0.2, 0.05 V (discharge), and 0.2 V (charge). The vertical dashed lines indicate the characteristic binding energies of the annotated compounds.

www.advancedsciencenews.com

ADVANCED ENERGY MATERIALS

www.advenergymat.de

conductivity and the ion transference in the SEI layer. During lithiation in Si  $\parallel$  Li metal cells, AlF<sub>3</sub> will be able to convert to LiF as already reported by Cui's group<sup>[44]</sup>

$$2AlF_3 + 3Li^+ + 3e^- \rightarrow Li_3AlF_6 + Al \quad E = 1.28 \text{ V vs. } Li \mid Li^+$$
 (1)

$$Li_{3}AlF_{6}+Al+3Li^{+}+3e^{-}\rightarrow6LiF+2Al~~E=1.06\,V~vs.~Li~|~Li^{+}$$

$$3\text{LiF} + \text{Al} + \text{Li}^+ + \text{e}^- \rightarrow 3\text{LiF} + \text{LiAl} \quad \text{E} = 0.36\text{V vs. Li} \mid \text{Li}^+$$
 (3)

(2)

$$3\text{LiF} + \text{LiAl} + 0.5\text{Li}^{+} + 0.5\text{e}^{-} \rightarrow 3\text{LiF} + 0.5\text{Li}_{3}\text{Al}_{2}$$
  
E = 0.19V vs. Li | Li<sup>+</sup> (4)

$$3\text{LiF} + 0.5\text{Li}_3\text{Al}_2 + 0.75\text{Li}^+ + 0.75\text{e}^- \rightarrow 3\text{LiF} + 0.25\text{Li}_9\text{Al}_4$$
  
 $E = 0.07\text{V vs. Li} \mid \text{Li}^+$  (5)

Based on the calculation above, these five degradation reactions that consume Li+ depend on the exact applied potential. Because Li-containing species (e.g., LiF, Li<sub>3</sub>AlF<sub>6</sub>, etc.) are produced in each step as the byproducts, the relative atomic concentration of Li species (from Li 1s core spectrum) of the coated Si is higher than for uncoated Si (Figure S10a, Supporting Information). The formed phases may have high intrinsic Li<sup>+</sup> ion conductivity and may show a porous morphology due to volume change upon phase transformation to facilitate Li+ ion transport across the film. For Al species (from Al 2p core spectrum), the atomic concentration is very low (<1 at%) due to the coverage from the inorganic and organic SEI layer on top of it. The signal is too low to be detected and to some extent might not be reliable. Therefore, the quantification on this Al 2p must be interpreted with caution (Figure S10b, Supporting Information).

To further confirm the formation of Li–Al–F compounds (e.g., Li<sub>3</sub>AlF<sub>6</sub>), ion chromatography with conductivity detection (IC-CD) was performed for "Si + 20 nm AlF<sub>3</sub>" after the 1st cycle (referred to as "cycled coated Si") as shown in **Figure 7**. For comparison, the uncycled "Si + 20 nm AlF<sub>3</sub>" after being

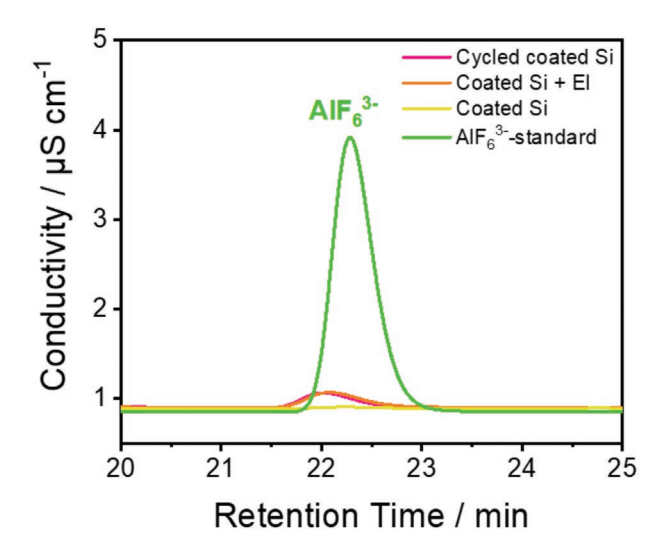


**Figure 7.** Ion chromatography with conductivity detection (IC-CD) profile for aluminium hexafluoride anion (AlF $_6$ <sup>3-</sup>).

exposed to the electrolyte (referred to as "coated Si + El") and pristine "Si + 20 nm AlF<sub>3</sub>" (referred to as "coated Si") were also measured. By using Na<sub>3</sub>AlF<sub>6</sub>, the peak location of the AlF<sub>6</sub><sup>3-</sup> was able to be detected after ≈22.2 min of retention time as a reference. In contrast to the "coated Si" electrode which does not show the peak of AlF<sub>6</sub><sup>3-</sup>, this peak is visible for the "cycled coated Si" electrode, thus, demonstrating the formation of Li-Al-F compounds from AlF<sub>3</sub> which most likely corresponds to Li<sub>3</sub>AlF<sub>6</sub> species. Interestingly, this peak was also found with comparable intensity in the "uncycled coated Si" demonstrating that the electrolyte exposure might be already sufficient to induce the transformation of AlF<sub>3</sub> to LiAlF<sub>6</sub> even before electrochemical cycling. This could mean that the AlF<sub>3</sub> coating would stabilize the interface since the very beginning, i.e., even before electrochemical operation, and act as "artificial SEI". The slight shift from the reference was probably due to the higher amount of AlF<sub>6</sub><sup>3-</sup>. After all, these results are in agreement with the XPS results to further verify that the generated Li-Al-F compounds might be the major reason for the improved cycling performance of coated Si thin film anodes.

We thus conclude that the addition of AlF<sub>3</sub> at the interface give beneficial effects for an effective SEI formation.[45] The schematic SEI formation in uncoated Si thin film electrodes and coated Si thin film electrodes is shown in Figure 8a,b. In coated Si thin film, the AlF<sub>3</sub> coating help in stabilizing the Silelectrolyte interface during cycling. The potential formation mechanism involves organic species on the top of the SEI during the lithiation process. At the same time, the transformation of AlF<sub>3</sub> to the Li-Al-F phase will produce an abundant amount of LiF which will inhibit the continuous SEI decomposition. The organic-inorganic SEI layer combined with the Li-Al-F thin layer is proposed to be strongly bonded to the Li<sub>x</sub>Si<sub>y</sub> surface, which makes the SEI less suffer from the high deformation during the alloying reaction. This will then minimize the breakage and/or reformation of the SEI upon cell operation. Once AlF<sub>3</sub> is lithiated, it also possesses relatively high ionic conductivity. Results reported herein open a new avenue toward the development of functional coatings on Si thin films, in an effort to improve the SEI properties. In a more practical cell format (e.g., by using a composite of Si particles in combination with graphite) with inactive materials involved (i.e., binder and conductive agent), other factors should be taken into account, such as the possible change of the specific surface area, the electronic conductivity, and the homogeniety of the coating on the surface of Si particles.

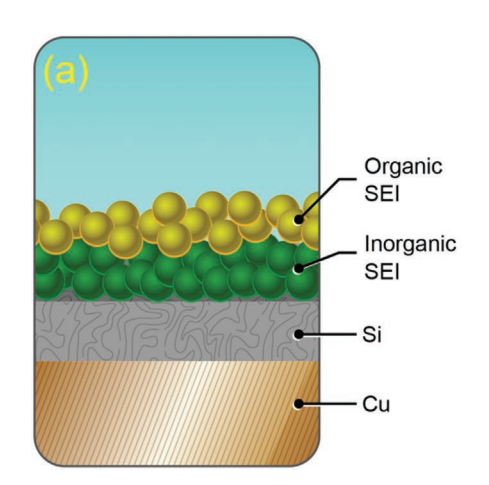
#### 3. Conclusion

In this study, thin AlF<sub>3</sub> coatings were employed on Si thin film to provide long-term protection at the interface. A comprehensive approach to evaluate the SEI formation under the impact of AlF<sub>3</sub> coating was presented by utilizing XPS in different (de-)lithiation states. 100 nm thick Si thin films were used as a model electrode. It was shown that with the addition of a thin layer (5 and 20 nm) of AlF<sub>3</sub>, the resistance is reduced and the cycling retention is significantly improved. The chemical compounds present on the surface of the electrodes during charge/discharge were semiquantitatively examined where the

16146840, 2022, 41, Downloaded from https://onlinelibrary.wiley.com/doi/10.1002/aenm.202201859 by Forschungszentrum Jülich GmbH Research Center, Wiley Online Library on [04/11/2022]. See the Terms

: (https://onlinelibrary.wiley.com/terms-and-conditions) on Wiley Online Library for rules of use; OA articles are governed by the applicable Creative Commons

www.advancedsciencenews.com www.advenergymat.de



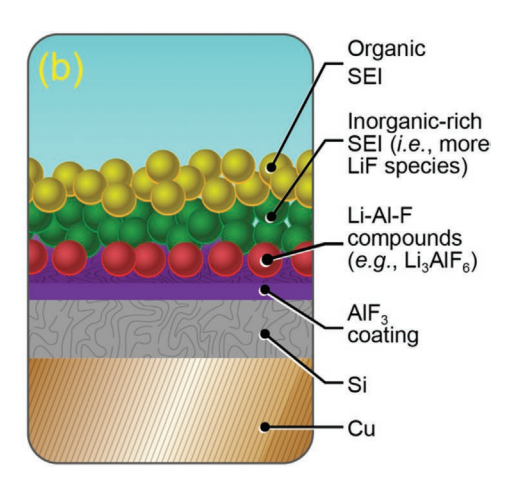


Figure 8. Schematic illustrations of the SEI on a) uncoated Si and b) coated Si electrodes. In coated Si electrodes, the SEI formation mechanism involves the transformation of AIF $_3$  to the Li–Al–F compounds (e.g., Li $_3$ AIF $_6$ ).

SEI in coated Si thin film contain LiF-rich species. The transformation of AlF<sub>3</sub> to highly Li<sup>+</sup> ion conductive Li—Al—F phases (e.g., Li<sub>3</sub>AlF<sub>6</sub>) was confirmed by utilizing IC-CD and is responsible for this enhancement in cycling performance. Further, this study suggests future directions to improve coating layer studies on Si anodes in future works, and help pave the way for developing high energy density LIB cells.

### **Supporting Information**

Supporting Information is available from the Wiley Online Library or from the author.

#### Acknowledgements

The authors thank the Ministry for Culture and Science of North-Rhine Westphalia (Germany) for funding this work within the International Graduate School for Battery Chemistry, Characterization, Analysis, Recycling and Application (BACCARA). E.A. would like to thank Dr. Suryaningtyas Margi Utami for her fantastic support. In addition, the authors greatly acknowledge Andre Bar for graphics support.

Open access funding enabled and organized by Projekt DEAL.

#### **Conflict of Interest**

The authors declare no conflict of interest.

#### **Data Availability Statement**

The data that support the findings of this study are available from the corresponding author upon reasonable request.

#### **Keywords**

 $\mathsf{AIF}_3$  coatings, delithiation, lithiation, silicon thin films, solid electrolyte interphase

Received: May 31, 2022 Revised: July 8, 2022 Published online: August 26, 2022

- T. Placke, R. Kloepsch, S. Dühnen, M. Winter, J. Solid State Electrochem. 2017. 21, 1939.
- [2] a) M. Winter, B. Barnett, K. Xu, Chem. Rev. 2018, 118, 11433;
  b) D. Andre, H. Hain, P. Lamp, F. Maglia, B. Stiasznya, J. Mater. Chem. A 2017, 5, 17174;
  c) E. Adhitama, P. C. Rath, A. Prayogi, J. Patra, T.-C. Lee, J. Li, J.-K. Chang, Carbon 2021, 184, 752.
- [3] E. Adhitama, F. Dias Brandao, I. Dienwiebel, M. M. Bela, A. Javed, L. Haneke, M. C. Stan, M. Winter, A. Gomez-Martin, T. Placke, Adv. Funct. Mater. 2022, 32, 2201455.
- [4] a) M. T. McDowell, S. W. Lee, W. D. Nix, Y. Cui, Adv. Mater. 2013, 25, 4966; b) M. N. Obroyac, V. L. Chevrier, Chem. Rev. 2014, 114, 11444.
- [5] M. Wetjen, M. Trunk, L. Werner, R. Gernhäuser, B. Märkisch, Z. Révay, R. Gilles, H. A. Gasteiger, J. Electrochem. Soc. 2018, 165, A2340
- [6] a) T. Placke, G. G. Eshetu, M. Winter, E. Figgemeier, in Lithium-Ion Batteries Enabled by Silicon Anodes, Vol. 11, (Eds: C. Ban, K. Xu), The Institution of Engineering and Technology (IET), London 2021, p. 349; b) C. Wölke, B. A. Sadeghi, G. G. Eshetu, E. Figgemeier, M. Winter, I. Cekic-Laskovic, Adv. Mater. Interfaces 2022, 9, 2101898; c) F. Holtstiege, A. Wilken, M. Winter, T. Placke, Phys. Chem. Chem. Phys. 2017, 19, 25905.
- [7] a) C. Liu, Z. G. Neale, G. Cao, Mater. Today 2016, 19, 109;
  b) P. Peljo, H. H. Girault, Energy Environ. Sci. 2018, 11, 2306;
  c) Z. Yan, M. N. Obrovac, J. Power Sources 2018, 397, 374.
- [8] G. Liu, S. Xun, N. Vukmirovic, X. Song, P. Olalde-Velasco, H. Zheng, V. S. Battaglia, L. Wang, W. Yang, Adv. Mater. 2011, 23, 4679.
- [9] M. Winter, Z. Phys. Chem. 2009, 223, 1395.
- [10] E. Peled, S. Menkin, J. Electrochem. Soc. 2017, 164, A1703.
- [11] a) I. Hasa, A. M. Haregewoin, L. Zhang, W.-Y. Tsai, J. Guo, G. M. Veith, P. N. Ross, R. Kostecki, ACS Appl. Mater. Interfaces 2020, 12, 40879; b) A. L. Michan, G. Divitini, A. J. Pell, M. Leskes, C. Ducati, C. P. Grey, J. Am. Chem. Soc. 2016, 138, 7918; c) Y. Yin, E. Arca, L. Wang, G. Yang, M. Schnabel, L. Cao, C. Xiao, H. Zhou, P. Liu, J. Nanda, G. Teeter, B. Eichhorn, K. Xu, A. Burrell, C. Ban, ACS Appl. Mater. Interfaces 2020, 12, 26593.
- [12] S. Krueger, R. Kloepsch, J. Li, S. Nowak, S. Passerini, M. Winter, J. Electrochem. Soc. 2013, 160, A542.
- [13] a) A. L. Michan, B. S. Parimalam, M. Leskes, R. N. Kerber, T. Yoon, C. P. Grey, B. L. Lucht, *Chem. Mater.* 2016, 28, 8149; b) K. Schroder, J. Alvarado, T. A. Yersak, J. Li, N. Dudney, L. J. Webb, Y. S. Meng, K. J. Stevenson, *Chem. Mater.* 2015, 27, 5531.
- [14] B. Umesh, P. Chandra Rath, R. F. H. Hernandha, J.-Y. Lin, S. B. Majumder, Q.-F. Dong, J.-K. Chang, ACS Sustainable Chem. Eng. 2020, 8, 16252.

ADVANCED SCIENCE NEWS

ADVANCED ENERGY MATERIALS

www.advancedsciencenews.com www.advenergymat.de

- [15] R. Jung, M. Metzger, D. Haering, S. Solchenbach, C. Marino, N. Tsiouvaras, C. Stinner, H. A. Gasteiger, J. Electrochem. Soc. 2016, 163, A1705.
- [16] H. T. Nguyen, M. R. Zamfir, L. D. Duong, Y. H. Lee, P. Bondavalli, D. Pribat, J. Mater. Chem. 2012, 22, 24618.
- [17] a) T. Feng, Y. Xu, Z. Zhang, X. Du, X. Sun, L. Xiong, R. Rodriguez, R. Holze, ACS Appl. Mater. Interfaces 2016, 8, 6512; b) D. Wang, J. Yang, J. Liu, X. Li, R. Li, M. Cai, T.-K. Sham, X. Sun, J. Mater. Chem. A 2014, 2, 2306.
- [18] S. Casino, B. Heidrich, A. Makvandi, T. Beuse, T. Gallasch, M. Peterlechner, G. Wilde, M. Winter, P. Niehoff, J. Energy Storage 2021, 44, 103479.
- [19] a) X. Zhang, I. Belharouak, L. Li, Y. Lei, J. W. Elam, A. Nie, X. Chen, R. S. Yassar, R. L. Axelbaum, Adv. Energy Mater. 2013, 3, 1299;
  b) S.-J. Kim, M.-C. Kim, D.-H. Kwak, D.-M. Kim, G.-H. Lee, H.-S. Choe, K.-W. Park, J. Power Sources 2016, 304, 119; c) S. J. Shi, J. P. Tu, Y. Y. Tang, X. Y. Liu, Y. Q. Zhang, X. L. Wang, C. D. Gu, Electrochim. Acta 2013, 88, 671; d) Y. K. Sun, Y. S. Lee, M. Yoshio, K. Amine, Electrochem. Solid-State Lett. 2002, 5, A99.
- [20] a) Z. Yang, Q. Qiao, W. Yang, Electrochim. Acta 2011, 56, 4791;
  b) H. J. Lee, Y. J. Park, Solid State Ion 2013, 230, 86; c) Y.-K. Sun, M.-J. Lee, C. S. Yoon, J. Hassoun, K. Amine, B. Scrosati, Adv. Mater. 2012, 24, 1192; d) Y. Zhou, Y. Lee, H. Sun, J. M. Wallas, S. M. George, M. Xie, ACS Appl. Mater. Interfaces 2017, 9, 9614.
- [21] a) Y. He, X. Yu, Y. Wang, H. Li, X. Huang, Adv. Mater. 2011, 23, 4938;
  b) B. Xiao, X. Sun, Adv. Energy Mater. 2018, 8, 1802057;
  c) I. Bloom,
  L. Trahey, A. Abouimrane, I. Belharouak, X. Zhang, Q. Wu, W. Lu,
  D. P. Abraham, M. Bettge, J. W. Elam, X. Meng, A. K. Burrell, C. Ban,
  R. Tenent, J. Nanda, N. Dudney, J. Power Sources 2014, 249, 509.
- [22] a) S. Xu, R. M. Jacobs, H. M. Nguyen, S. Hao, M. Mahanthappa,
   C. Wolvertond, D. Morgan, J. Mater. Chem. A 2015, 3, 17248;
   b) S. Hao, C. Wolverton, J. Phys. Chem. C 2013, 117, 8009.
- [23] D. Peralta, J. Salomon, Y. Reynier, J.-F. Martin, E. De Vito, J.-F. Colin, A. Boulineau, C. Bourbon, B. Amestoy, C. Tisseraud, R. Pellenc, J.-L. Ferrandis, D. Bloch, S. Patoux, *Electrochim. Acta* 2021, 400, 139419.
- [24] C. M. Julien, A. Mauger, AIMS Mater. Sci. 2019, 6, 406.
- [25] a) J.-H. Kim, M.-S. Park, J.-H. Song, D.-J. Byun, Y.-J. Kim, J.-S. Kim, J. Alloys Compd. 2012, 517, 20; b) T. Oi, K. Miyauchi, K. Uehara, J. Appl. Phys. 1982, 53, 1823.
- [26] a) F. Ding, W. Xu, D. Choi, W. Wang, X. Li, M. H. Engelhard, X. Chen, Z. Yang, J.-G. Zhang, J. Mater. Chem. 2012, 22, 12745; b) H. Park, S. Choi, S. Lee, G. Hwang, N.-S. Choi, S. Park, J. Mater. Chem. A 2015, 3, 1325.

- [27] L. Tong, P. Wang, W. Fang, X. Guo, W. Bao, Y. Yang, S. Shen, F. Qiu, ACS Appl. Mater. Interfaces 2020, 12, 29242.
- [28] J. O. Besenhard, M. W. Wagner, M. Winter, A. D. Jannakoudakis, P. D. Jannakoudakis, E. Theodoridou, J. Power Sources 1993, 44, 413.
- [29] M. S. Park, G. X. Wang, H. K. Liu, S. X. Dou, Electrochim. Acta 2006, 51, 5246.
- [30] J. Sun, X. Li, W. Zhang, K. Yi, J. Shao, Appl. Opt. 2012, 51, 8481.
- [31] a) A. Makarowicz, C. L. Bailey, N. Weiher, E. Kemnitz, S. L. M. Schroeder, S. Mukhopadhyay, A. Wander, B. G. Searle, N. M. Harrison, *Phys. Chem. Chem. Phys.* 2009, 11, 5664; b) M. Mäntymäki, M. J. Heikkilä, E. Puukilainen, K. Mizohata, B. Marchand, J. Räisänen, M. Ritala, M. Leskelä, *Chem. Mater.* 2015, 27, 604.
- [32] G. I. Ashok Kumar, A. Lambert, J. Caperton, M. Asokan, W. Yi, O. Chyan, Corros. Mater. Degrad. 2021, 2, 447.
- [33] A. Buchheit, M. Hoffmeyer, B. Teßmer, K. Neuhaus, J. Electrochem. Soc. 2021, 168, 010531.
- [34] a) X. Zhu, R. I. Revilla, A. Hubin, J. Phys. Chem. C 2018, 122, 28556;
  b) J. Wu, S. Yang, W. Cai, Z. Bi, G. Shang, J. Yao, Sci. Rep. 2017, 7, 11164.
- [35] C. Örnek, C. Leygraf, J. Pan, Corros. Eng. Sci. Technol. 2019, 54, 185.
- [36] a) Q. Wu, B. Shi, J. Bareño, Y. Liu, V. A. Maroni, D. Zhai,
  D. W. Dees, W. Lu, ACS Appl. Mater. Interfaces 2018, 10, 3487;
  b) J. Li, A. K. Dozier, Y. Li, F. Yang, Y.-T. Cheng, J. Electrochem. Soc. 2011, 158, A689.
- [37] a) H. Jung, M. Park, Y.-G. Yoon, G.-B. Kim, S.-K. Joo, J. Power Sources 2003, 115, 346; b) J. P. Maranchi, A. F. Hepp, P. N. Kumta, Electrochem. Solid-State Lett. 2003, 6, A198.
- [38] A. R. Jiménez, R. Klöpsch, R. Wagner, U. C. Rodehorst, M. Kolek, R. Nölle, M. Winter, T. Placke, ACS Nano 2017, 11, 4731.
- [39] a) R. Nölle, J.-P. Schmiegel, M. Winter, T. Placke, Chem. Mater. 2019, 32, 173; b) R. Nölle, A. J. Achazi, P. Kaghazchi, M. Winter, T. Placke, ACS Appl. Mater. Interfaces 2018, 10, 28187.
- [40] F. Aupperle, G. G. Eshetu, K. W. Eberman, A. Xioa, J.-S. Bridelf, E. Figgemeier, J. Mater. Chem. A 2020, 8, 19573.
- [41] B. Heidrich, M. Börner, M. Winter, P. Niehoff, J. Energy Storage 2021, 44, 103208.
- [42] H. Kobayashi, G. Yuan, Y. Gambe, I. Honma, ACS Appl. Energy Mater. 2021. 4, 9866.
- [43] X. Xiao, P. Lu, D. Ahn, Adv. Mater. 2011, 23, 3911.
- [44] J. Xie, A. D. Sendek, E. D. Cubuk, X. Zhang, Z. Lu, Y. Gong, T. Wu, F. Shi, W. Liu, E. J. Reed, Y. Cui, ACS Nano 2017, 11, 7019.
- [45] E. Markevich, G. Salitra, D. Aurbach, ACS Energy Lett. 2017, 2, 1337.